

## Magnetically Separable FeO/TiO Hollow Spheres: Fabrication and Photocatalytic Activity

Shouhu Xuan, Wanquan Jiang, Xinglong Gong, Yuan Hu, and Zuyao Chen

*J. Phys. Chem. C*, **2009**, 113 (2), 553-558 • DOI: 10.1021/jp8073859 • Publication Date (Web): 18 December 2008

Downloaded from <http://pubs.acs.org> on March 30, 2009

### More About This Article

---

Additional resources and features associated with this article are available within the HTML version:

- Supporting Information
- Access to high resolution figures
- Links to articles and content related to this article
- Copyright permission to reproduce figures and/or text from this article

[View the Full Text HTML](#)

# Magnetically Separable Fe<sub>3</sub>O<sub>4</sub>/TiO<sub>2</sub> Hollow Spheres: Fabrication and Photocatalytic Activity

Shouhu Xuan,<sup>†,‡</sup> Wanquan Jiang,<sup>‡</sup> Xinglong Gong,<sup>§</sup> Yuan Hu,<sup>\*,†</sup> and Zuyao Chen<sup>‡</sup>

State Key laboratory of Fire Science, Department of Chemistry, and CAS Key Laboratory of Mechanical Behavior and Design of Materials, Department of Mechanics and Mechanical Engineering, The University of Science and Technology of China, Hefei, Anhui, 230026, People's Republic of China

Received: August 18, 2008; Revised Manuscript Received: November 10, 2008

Well-defined magnetic separable, hollow spherical Fe<sub>3</sub>O<sub>4</sub>/TiO<sub>2</sub> hybrid photocatalysts were successfully prepared through a poly(styrene–acrylic acid) (PSA) template method. This bifunctional product was characterized in terms of the particle size, surface morphology, chemical composition, and magnetic properties using transmission electron microscopy (TEM), field emission scanning electron microscopy (FE-SEM), and X-ray powder diffraction (XRD) patterns. The *M*–*H* hysteresis loop for Fe<sub>3</sub>O<sub>4</sub>/TiO<sub>2</sub> hollow spheres indicates that the composite spheres show superparamagnetic characteristics at room temperature. These magnetic TiO<sub>2</sub> composites with hollow nature exhibit good photocatalytic activity under UV light irradiation and can be recycled six times by magnetic separation without major loss of activity. This method can be further applied to synthesize other bifunctional hollow spheres, such as Fe<sub>3</sub>O<sub>4</sub>/SnO<sub>2</sub> and Fe<sub>3</sub>O<sub>4</sub>/CdS.

## 1. Introduction

Oxide semiconductor mediated photocatalytic purification of polluted air and wastewater is a promising environmental remediation technology, especially for low levels of organic contaminants.<sup>1</sup> Among various oxide semiconductor photocatalysts, TiO<sub>2</sub><sup>2–5</sup> has proven to be the most suitable material for widespread environmental application for its biological and chemical inertness, strong oxidizing power, cost effectiveness, and long-term stability against photocorrosion and chemical corrosion. Nanostructured TiO<sub>2</sub> exhibits superior photocatalytic activity compared to conventional bulk material because of its high surface area and is one of the most intensively researched substances of the past decade. To enhance its photocatalytic ability, nanostructured TiO<sub>2</sub> with various morphologies including nanoparticles, nanofibers, nanostructured films or coatings, and nanotubes have been prepared, and much progress on the synthesis of nanostructured TiO<sub>2</sub> with excellent catalytic properties has been made.<sup>6–9</sup>

Typically, a photocatalytic reaction is conducted in a suspension of submicrometer semiconductor materials, and therefore the conventional TiO<sub>2</sub> catalysts would inevitably encounter an obstacle when applied in practice, that is, the difficulties in separation and manipulation due to their small size. Removing such tiny particles from large volumes of water involves further expense. This presents a major drawback to the application of the photocatalytic processes for treating wastewaters. Previous research stated that,<sup>10</sup> due to the small particle size of the catalyst used, the cost requirements for this downstream separation may even invalidate altogether the claimed energy savings for a solar-induced decontamination process. Although the preassembly of TiO<sub>2</sub> nanoparticles on an appropriate substrate may partially solve this problem under some circumstances, a high dispersibility and a good manipulability of TiO<sub>2</sub> nanocrystals were the premises of some important applications.

Magnetic separation provides a very convenient approach for removing and recycling magnetic particles/composites by applying an appropriate magnetic field. This approach may prevent the agglomeration of the catalyst particles during recovery and can increase the durability of the catalysts. Catalysts have been immobilized on various magnetic supports, including polymers,<sup>11</sup> carbon,<sup>12</sup> and silica,<sup>13</sup> and other nanocomposites combining mesoporous materials with a high surface area and well-defined pore size with magnetic nanoparticles.<sup>14</sup> Fortunately, research has been carried out by immobilizing TiO<sub>2</sub> onto various magnetic supports, such as magnetite,<sup>15</sup> ferrite,<sup>16</sup> barium ferrite,<sup>17</sup> and Fe<sub>3</sub>O<sub>4</sub>@SiO<sub>2</sub> particles.<sup>18</sup> These magnetic photocatalysts can not only be recovered but also fluidized by applying an external magnetic field. However, most works in this area have focused on a solid spherical shape, and the resulting magnetic photocatalysts are not uniform in size. Therefore, the synthesis of magnetic TiO<sub>2</sub> nanoparticles with both hollow nature and uniform size has become a pressing need not only for the fundamental interest but also for their high efficiency and facility.

As a unique class of structured materials, hollow colloidal particles have attracted growing research efforts owing to their technological importance in a wide range of applications.<sup>19</sup> Thanks to many years of efforts from various groups, many strategies have been developed to fabricate and apply TiO<sub>2</sub> particles with hollow interiors as photocatalysts.<sup>20</sup> However, although TiO<sub>2</sub> hollow spheres equipped with functional microparticles in their cavities have been developed by some groups,<sup>21</sup> there are few reports about the fabrication of hollow TiO<sub>2</sub> with magnetic particles inside.<sup>22</sup>

A template against colloid particles is probably the most effective and general method for the preparation of hollow particles,<sup>23,24</sup> especially for studies in which a narrow size distribution is required, for example, self-assembly and photonic crystals. Monodisperse poly(styrene–acrylic acid) (PSA) latex and silica spheres are commonly used as colloidal templates because they are readily available in a wide range of sizes. The apparent advantage of the template method is that the shape

\* Corresponding author. Telephone: +86 551 3601664. Fax: +86 551 3601664. E-mail: yuanhu@ustc.edu.cn.

<sup>†</sup> State Key laboratory of Fire Science.

<sup>‡</sup> Department of chemistry.

<sup>§</sup> Department of Mechanics and Mechanical Engineering.

and cavity size of formed hollow structures are directly determined by the template.

From this viewpoint, we propose a flexible process for fabricating magnetic hollow  $\text{TiO}_2$  spheres by using a PSA template method. This route is useful to obtain interesting and controllable structural hollow  $\text{TiO}_2$  spheres with magnetic  $\text{Fe}_3\text{O}_4$  particles inside. To the best of our knowledge, this is the first report about a hollow sphere-like magnetic  $\text{Fe}_3\text{O}_4/\text{TiO}_2$  hybrid photocatalyst. These results offer a powerful platform to construct other magnetic hollow spheres applied in catalysis.

## 2. Experimental Section

**Materials.** Ferric chloride hexahydrate ( $\text{FeCl}_3 \cdot 6\text{H}_2\text{O}$ ), sodium sulfite anhydrous ( $\text{Na}_2\text{SO}_3$ ), titanium butoxide (TBOT), acrylic acid monomer (AA), and rhodamine B (RhB) were from Sinopharm Chemical Reagent Co, Ltd. Ammonium hydroxide ( $\text{NH}_3 \cdot \text{H}_2\text{O}$ , 25%–28%) was from Lingfeng Chemical Reagent Co, Ltd. of Shanghai. All these reagents were used as received without further purification. Styrene from Shanghai Chemical Reagents Company was washed using 5 wt % sodium hydroxide solution first and then with distilled water three times and stored at 4 °C. Doubly deionized water was used through all the processes.

**Synthesis of PSA Spheres.** Monodispersed PSA latex spheres have been synthesized in our group by emulsion copolymerization.<sup>25</sup> Briefly, styrene and acrylic acid monomer (their weight ratio is 100:2) were copolymerized in the emulsion using sodium dodecyl sulfate (SDS) as the surfactant and ammonium persulfate (APS) as initiator. The reaction was carried out in nitrogen at 70 °C for 12 h under mechanical stirring at 350 rpm. The latex was purified by three centrifugation/dispersion cycles in water.

**Synthesis of PSA/ $\text{Fe}_3\text{O}_4$  Composite Spheres.** A 0.5 g sample of monodispersed PSA latex spheres (270 nm in diameter) was dispersed in 150 mL of aqueous ethanol (1:2, v/v) solution via ultrasound. Then, 50 mL of the above solution was added to 100 mL of water containing  $6 \times 10^{-4}$  M  $\text{FeCl}_3$ . The suspension was allowed to stand for 1 day to ensure the surface of the PSA spheres was sufficiently adsorbed by  $\text{Fe}^{3+}$  ions. Following this, the solution was placed in a 250 mL three-necked round-bottom flask under  $\text{N}_2$  atmosphere to minimize the amount of dissolved oxygen. After purging with high-purity  $\text{N}_2$  gas for at least 1/2 h, the pH of the mixture was adjusted to 9 or 10 by means of  $\text{NH}_3 \cdot \text{H}_2\text{O}$ . Ten minutes later, an aqueous solution of  $\text{Na}_2\text{SO}_3$  (10 mL,  $1 \times 10^{-4}$  M) was added under  $\text{N}_2$ . The mixture was kept stirring at 40 °C for a further 4 h. At the end of the reaction the particles were magnetically separated from the reaction medium and washed several times each with water and ethanol. The microspheres were dried under vacuum at 50 °C overnight.

**Synthesis of PSA@ $\text{Fe}_3\text{O}_4/\text{Ti}(\text{OH})_x$  Core/Shell Spheres.** A 0.1 g sample of as-prepared PSA/ $\text{Fe}_3\text{O}_4$  composite particles was dispersed in a 55 mL mixture of *n*-butyl alcohol and ethanol (10:1, v/v) in an ultrasonic bath. Sixty minutes later, this suspension was transferred into a reaction vessel and kept at 25 °C. A predetermined amount of TBOT (0.2 mL) was dissolved in 10 mL of ethanol and added to the above mixture. Then, the solution was stirred overnight to allow a saturated adsorption of TBOT on the shell of the composite particles. After that, 10 mL of aqueous ethanol (3:7, v/v) was added to the mixture and held for 12 h. The amorphous  $\text{TiO}_2$  coated magnetic composite spheres (PSA@ $\text{Fe}_3\text{O}_4/\text{Ti}(\text{OH})_x$ ) were washed three times with ethanol, followed by two times with water. These particles were dried in the vacuum oven at 50 °C for 12 h.

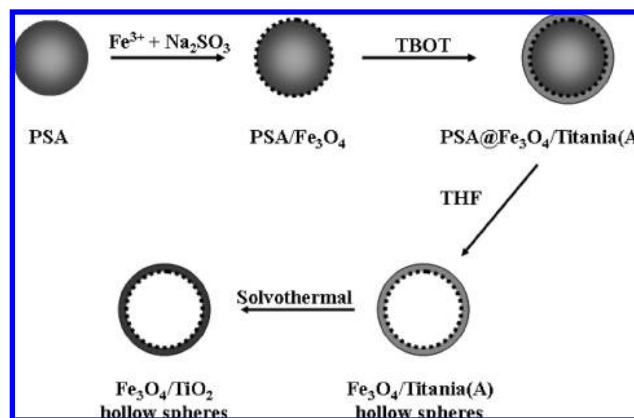


**Figure 1.** Schematic procedure used for fabrication of magnetic  $\text{TiO}_2$  hollow spheres (A: amorphous).

**Synthesis of  $\text{Fe}_3\text{O}_4/\text{TiO}_2$  Hollow Spheres.** The  $\text{Fe}_3\text{O}_4/\text{Ti}(\text{OH})_x$  hollow spheres were prepared by dissolving PSA cores from the PSA@ $\text{Fe}_3\text{O}_4/\text{Ti}(\text{OH})_x$  particles in THF. Later, the  $\text{Fe}_3\text{O}_4/\text{Ti}(\text{OH})_x$  hollow particles were dispersed in a certain amount of ethanol and the solution was transferred and sealed in a Teflon-sealed autoclave. The autoclave was kept at 160 °C for 3 h before being cooled in air naturally. The final  $\text{Fe}_3\text{O}_4/\text{TiO}_2$  hollow spheres were separated from the reaction medium by magnetic separation. Rinsing by water and ethanol was required before oven drying at 50 °C for 12 h.

**Photocatalytic Activity Measurement of  $\text{Fe}_3\text{O}_4/\text{TiO}_2$  Hollow Spheres.** The photocatalytic activities of the samples were evaluated by the degradation of RhB in an aqueous solution. Twenty-five milligrams of  $\text{Fe}_3\text{O}_4/\text{TiO}_2$  photocatalyst was suspended in 60 mL of RhB aqueous solution ( $1 \times 10^{-5}$  M). The solution was continuously stirred for about 1 h in the dark to ensure the establishment of an adsorption–desorption equilibrium among the photocatalyst, RhB, and water. Then the solution was exposed to UV irradiation from a 250-W high-pressure Hg lamp at room temperature. The samples were collected every 10 min to measure the RhB degradation by UV–vis spectra.

**Characterization.** X-ray powder diffraction (XRD) patterns of the products were obtained on a Japan Rigaku DMax- $\gamma$ A rotation anode X-ray diffractometer equipped with graphite monochromatized Cu K $\alpha$  radiation ( $\lambda = 1.54178$  Å). Transmission electron microscopy (TEM) photographs were taken on a Hitachi Model H-800 TEM at an accelerating voltage of 200 kV. The field emission scanning electron microscopy (FE-SEM) images were taken on a JEOL JSM-6700F SEM. X-ray photoelectron spectra (XPS) were measured on an ESCA Laboratory MKII instrument with Mg K $\alpha$  radiation as the exciting source. Their magnetic properties ( $M$ – $H$  curve) were measured at room temperature on a MPMS XL magnetometer made by Quantum Design Corp. The UV–vis spectra were registered by a UV-365 spectrophotometer.

## 3. Results and Discussion

The procedure employed to obtain  $\text{Fe}_3\text{O}_4/\text{TiO}_2$  hollow spheres is illustrated in Figure 1. First, monodispersed PSA latex spheres with average particle size  $\sim 270$  nm were initially synthesized by the emulsion copolymerization method. Then, as-prepared PSA templates were modified by  $\text{Fe}_3\text{O}_4$  to make them magnetically functionalized. The resultant PSA/ $\text{Fe}_3\text{O}_4$  composites were immersed into the solution of TBOT in a mixture of *n*-butyl alcohol and ethanol, and hydrolyzed to allow a shell of

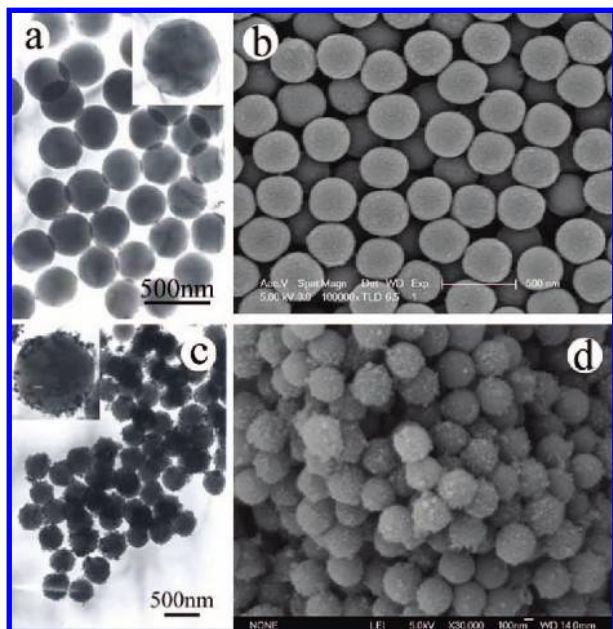


**Figure 2.** TEM and SEM images of PSA spheres (a, b) and PSA/Fe<sub>3</sub>O<sub>4</sub> spheres (c, d).

amorphous TiO<sub>2</sub> to form. Consequently, the above procedure results in the formation of uniform PSA@Fe<sub>3</sub>O<sub>4</sub>/Ti(OH)<sub>x</sub> core/shell spheres. After the PSA cores were removed from the capsules by dissolution with THF, Fe<sub>3</sub>O<sub>4</sub>/Ti(OH)<sub>x</sub> hollow spheres were obtained. Finally, as-prepared hollow spheres turned out to be highly crystallized by hydrothermal treatment to produce Fe<sub>3</sub>O<sub>4</sub>/TiO<sub>2</sub> hybrid hollow spheres. The thickness of TiO<sub>2</sub> shells and the size of cavities can be controlled through changing the TBOT content and the size of the PSA latex, as mentioned by Yang and co-workers.<sup>26</sup>

PSA has been of considerable interest because it forms the basis of technologically important materials. In our previous work,<sup>25</sup> we have synthesized monodispersed and well-defined spherical PSA spheres with a uniform size of 270 nm (Figure 2a) by emulsion copolymerization method. The as-prepared PSA spheres are hydrophilic and negatively charged because of carboxyl groups on the surface, which make it very easy to deposit a layer of Fe<sub>3</sub>O<sub>4</sub> nanoparticles on the surface of PSA spheres through a simple in situ solution method.<sup>27</sup>

Figure 2 displays TEM and SEM images of the pristine and Fe<sub>3</sub>O<sub>4</sub> attached PSA spheres, distinctively showing that PSA surfaces are uniformly coated by Fe<sub>3</sub>O<sub>4</sub> nanoparticles (Figure 2c). High-resolution TEM of the PSA/Fe<sub>3</sub>O<sub>4</sub> particles (inset of Figure 2c) reveals that the average size of Fe<sub>3</sub>O<sub>4</sub> particles is about 10 nm. Although these Fe<sub>3</sub>O<sub>4</sub> particles are irregularly dispersed on the PSA surface, only a few of them aggregated together. The SEM images of the PSA/Fe<sub>3</sub>O<sub>4</sub> particles (Figure 2d) also support that PSA cores are well coated by a noncontinuous layer of Fe<sub>3</sub>O<sub>4</sub> nanoparticles. Compared to the prime PSA cores (Figure 2b), the outside surfaces become coarse after the decorating process, indicating that Fe<sub>3</sub>O<sub>4</sub> nanoparticles are successfully loaded onto the surfaces of all PSA spheres. Figure 3a shows the typical XRD pattern of the obtained PSA/Fe<sub>3</sub>O<sub>4</sub> composite particles. All of the observed peaks in the pattern can be indexed to the face-centered-cubic phase of Fe<sub>3</sub>O<sub>4</sub> (JCPDS No. 19-629). No impurity is observed, which indicates that the product is pure Fe<sub>3</sub>O<sub>4</sub> phase. In addition, the broad peak appearing in the range from 15° to 25° indicates the existence of amorphous PSA. These XRD data also suggest that the PSA latexes were coated by the Fe<sub>3</sub>O<sub>4</sub> nanoparticles.

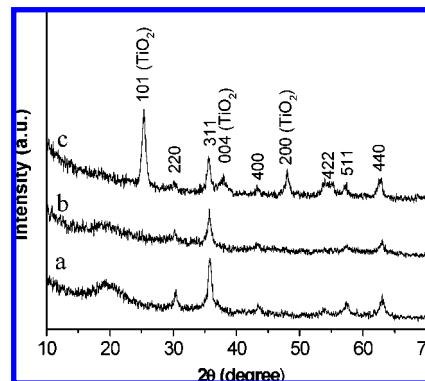


**Figure 3.** XRD patterns of the product PSA/Fe<sub>3</sub>O<sub>4</sub> spheres (a), PSA@Fe<sub>3</sub>O<sub>4</sub>/Ti(OH)<sub>x</sub> core/shell spheres (b), and Fe<sub>3</sub>O<sub>4</sub>/TiO<sub>2</sub> hollow spheres (c).

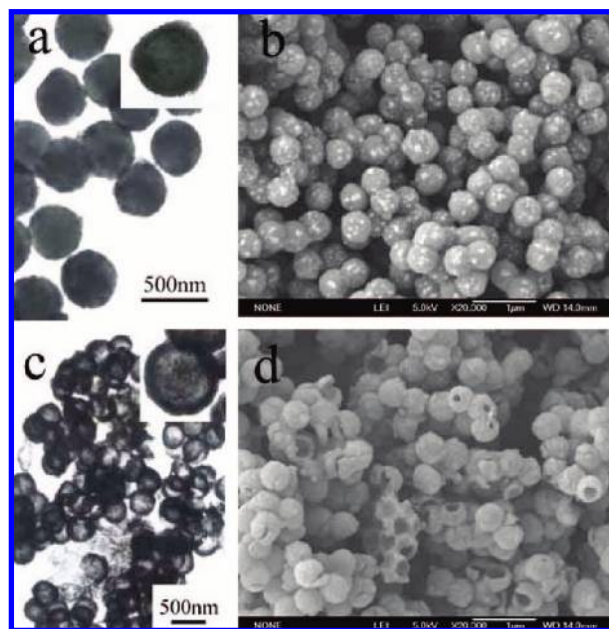


**Figure 4.** TEM and SEM images of PSA@Fe<sub>3</sub>O<sub>4</sub>/Ti(OH)<sub>x</sub> core/shell spheres (a, b) and Fe<sub>3</sub>O<sub>4</sub>/Ti(OH)<sub>x</sub> hollow spheres (c, d).

The PSA/Fe<sub>3</sub>O<sub>4</sub> hybrid particles were reused as a template for the selective loading of titanium compound. According to a previous report,<sup>27</sup> there are large amounts of functional groups on the surface of PSA, which enhance the affinity between the spheres and the prehydrolyzed TBOT. Figure 4a,b demonstrates the morphology of the obtained composite spheres. It could be seen that a well-defined core/shell structure with a PSA bead as the core and amorphous TiO<sub>2</sub> precursor (Ti(OH)<sub>x</sub>) as the shell was indeed formed (Figure 4a). The average diameter of the core/shell-like PSA@Fe<sub>3</sub>O<sub>4</sub>/Ti(OH)<sub>x</sub> particles was around 400 nm, which was also in agreement with SEM (Figure 4b), indicating that PSA/Fe<sub>3</sub>O<sub>4</sub> particles were covered completely by the Ti(OH)<sub>x</sub> shell. The inset of Figure 4a shows the representative TEM image of a single core/shell sphere. The size of the PSA core was maintained before and after the coating progress. The Ti(OH)<sub>x</sub> shells are about 60 nm in thickness, and no individually separated Ti(OH)<sub>x</sub> particles are observed in the sample, indicating that all the Ti(OH)<sub>x</sub> is loaded on the surfaces of the PSA/Fe<sub>3</sub>O<sub>4</sub> spheres. The outside surfaces of the PSA@Fe<sub>3</sub>O<sub>4</sub>/Ti(OH)<sub>x</sub> particles are very smooth compared to the PSA/Fe<sub>3</sub>O<sub>4</sub> particles. Additionally, between the Ti(OH)<sub>x</sub> shell and the PSA core, there exists a noncontinuous layer which is composed of Fe<sub>3</sub>O<sub>4</sub> nanoparticles (inset of Figure 4a).

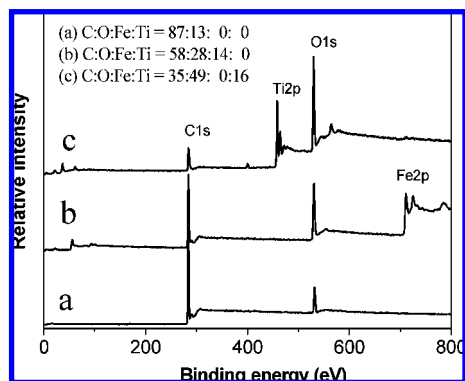


**Figure 5.** XPS spectra of PSA spheres (a), PSA/Fe<sub>3</sub>O<sub>4</sub> spheres (b), and PSA@Fe<sub>3</sub>O<sub>4</sub>/Ti(OH)<sub>x</sub> core/shell spheres (c).

In order to further understand the composition of these particles' surface, XPS of the samples was measured. The XPS spectra of bare PSA spheres, PSA/Fe<sub>3</sub>O<sub>4</sub> composite spheres, and PSA@Fe<sub>3</sub>O<sub>4</sub>/Ti(OH)<sub>x</sub> core/shell structured materials are shown in Figure 5. For PSA (Figure 5a), the main peaks are C 1s and O 1s centered at 285 and 532 eV. In the PSA/Fe<sub>3</sub>O<sub>4</sub> spectrum (Figure 5b), new peaks appear at 711 and 725 eV, assigned to photoelectrons originating from the Fe 2p energy level, which respond to the Fe element on the surface of PSA spheres. Figure 5c shows the XPS survey spectra of PSA@Fe<sub>3</sub>O<sub>4</sub>/Ti(OH)<sub>x</sub> core/shell particles. The core/shell particles exhibit a new Ti 2p peak (458 eV) which is very distinct from that of the PSA spheres and PSA/Fe<sub>3</sub>O<sub>4</sub> composites. This signal, which is not observed in the other two spectra, is in response to the Ti(OH)<sub>x</sub> coating layer. Furthermore, new minor peak appearing at 400 eV was attributed to the binding energy of chemisorbed N<sub>2</sub> molecules.<sup>28</sup> Compared to PSA/Fe<sub>3</sub>O<sub>4</sub>, the Fe signal is absent from this survey spectrum, indicating that the underlying Fe<sub>3</sub>O<sub>4</sub> is not probed by XPS. As XPS is a highly surface-specific technique with a typical analysis depth of ~10 nm (clearly lower than the thickness of the Ti(OH)<sub>x</sub> shell, ca. 60 nm), it is reasonable that Fe<sub>3</sub>O<sub>4</sub> is not detected. This thus provides experimental proof of the uniformity of the Ti(OH)<sub>x</sub> layer coating the magnetic PSA/Fe<sub>3</sub>O<sub>4</sub> particle cores. It is noteworthy that the intensity ratio of O 1s/C 1s has been multiplied by more than 5 compared to the uncoated PSA/Fe<sub>3</sub>O<sub>4</sub> particle. The drastic change of the O 1s/C 1s intensity ratio from PSA@Fe<sub>3</sub>O<sub>4</sub>/Ti(OH)<sub>x</sub> to PSA@Fe<sub>3</sub>O<sub>4</sub> provides strong evidence that the surface of this material is essentially Ti(OH)<sub>x</sub>. Therefore, the XPS data successfully verified that the PSA@Fe<sub>3</sub>O<sub>4</sub> has been well coated by the Ti(OH)<sub>x</sub> shell.

Figure 4c,d shows micrographs of the hollow Fe<sub>3</sub>O<sub>4</sub>/Ti(OH)<sub>x</sub> spheres after THF etching of the PSA@Fe<sub>3</sub>O<sub>4</sub>/Ti(OH)<sub>x</sub> core/shell particles. It is worth noting that the hollow structure and spherical shape are essentially preserved. The TEM image in Figure 4c shows a reduced electron density of the spheres compared to the corresponding unetched samples (Figure 4a), which can be assigned to the formation of a hollow structure. A wall thickness of ca. 60 nm for the Fe<sub>3</sub>O<sub>4</sub>/Ti(OH)<sub>x</sub> composite coating was estimated from Figure 4c by measuring the dark ring on the perimeter of the hollow spheres. The broken spheres in the SEM image (Figure 4d) further verified the well-defined hollow Fe<sub>3</sub>O<sub>4</sub>/Ti(OH)<sub>x</sub> hybrid spheres that were effectively formed after the removal of the PSA core by THF.

It is easy to understand that the titanium compound in the Fe<sub>3</sub>O<sub>4</sub>/Ti(OH)<sub>x</sub> hybrid hollow spheres is an X-ray amorphous essence. Therefore, the solvothermal method was conducted to make the amorphous precursor crystallize. Figure 3c shows the

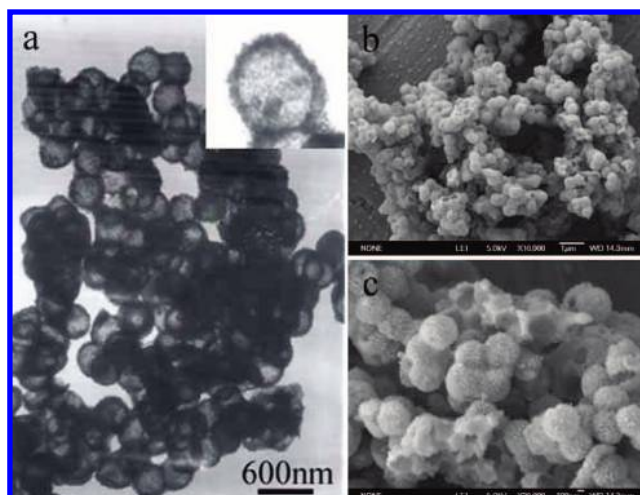


**Figure 6.** TEM and SEM images of Fe<sub>3</sub>O<sub>4</sub>/TiO<sub>2</sub> hollow spheres.

typical XRD patterns of the Fe<sub>3</sub>O<sub>4</sub>/TiO<sub>2</sub> hybrid hollow spheres. All the diffraction peaks in the pattern can be easily indexed to the cubic phase of Fe<sub>3</sub>O<sub>4</sub> (JCPDS No. 19-629) and anatase TiO<sub>2</sub> (JCPDS No. 21-1272). All the diffraction sharp peaks of Fe<sub>3</sub>O<sub>4</sub> were maintained after the coating process, which indicated that the effects on the crystal structure of Fe<sub>3</sub>O<sub>4</sub> nanoparticles were negligible during the present synthetic route. The XRD patterns indicate that the solvothermal treatment made the amorphous Ti(OH)<sub>x</sub> precursor completely transformed to crystalline TiO<sub>2</sub> with high phase purity. The average size of the TiO<sub>2</sub> crystallites was deduced by applying the Scherrer equation to the main peak (101), to give 10 nm.

The TEM images of the final Fe<sub>3</sub>O<sub>4</sub>/TiO<sub>2</sub> hollow spheres are shown in Figure 6. The obvious difference in color contrast between the central region and the verge presented a hollow spherical structure with a ~50 nm wall thickness. In the high-magnification TEM image (inset of Figure 6a), we could apparently observe the shell composed of nanoparticles of about 10 nm, which supported the XRD data. The shell is thinner than the amorphous one, which may be responding to the solvothermal treatment. The SEM image (Figure 6b) showed not only that the obtained Fe<sub>3</sub>O<sub>4</sub>/TiO<sub>2</sub> hollow particles retained their spherical morphology even after the solvothermal treatment but also that their surface was quite even and dense. As shown in Figure 6c, the hollow structure is clearly revealed from the broken spheres.

Superparamagnetism is the responsiveness to an applied magnetic field without retaining any magnetism after removal of the applied magnetic field. With the superparamagnetic property, capillary blockage by aggregations formed by residual magnetism after removal of the applied field will be avoided. The size of the Fe<sub>3</sub>O<sub>4</sub> component in our product is about 10 nm; therefore, it is reasonable to suppose that the hollow spheres will show superparamagnetic behavior. The magnetic behavior of the magnetic hollow particles was investigated using a superconducting quantum interference device magnetometer. The *M*–*H* curve (Figure 7) measurements of the sample indicate that the products inherit the superparamagnetic property from the Fe<sub>3</sub>O<sub>4</sub> nanoparticles, and its saturation magnetization value (*M*<sub>s</sub>) is about 12.8 emu/g. Taking into account that the sample contains 30% Fe<sub>3</sub>O<sub>4</sub> (ICP analysis data not shown), this gives a value of 42.7 emu/g. The *M*<sub>s</sub> is much lower than that of the corresponding bulk Fe<sub>3</sub>O<sub>4</sub> (92 emu/g),<sup>29</sup> which may be due to the small size of the Fe<sub>3</sub>O<sub>4</sub> nanoparticles.

To evaluate the photocatalytic activity of Fe<sub>3</sub>O<sub>4</sub>/TiO<sub>2</sub> hybrid hollow spherical photocatalyst, RhB dye solution was used as

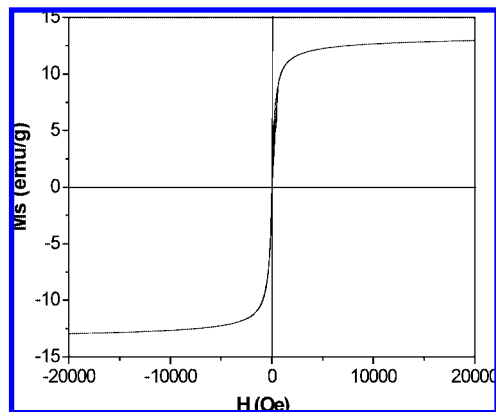


Figure 7.  $M-H$  curve of Fe<sub>3</sub>O<sub>4</sub>/TiO<sub>2</sub> hollow spheres at room temperature.

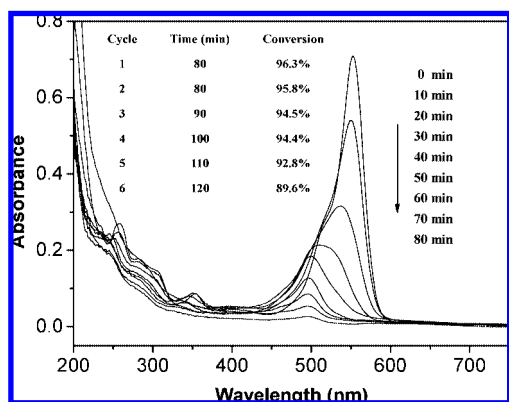


Figure 8. UV-vis spectral changes of RhB aqueous solution in the presence of Fe<sub>3</sub>O<sub>4</sub>/TiO<sub>2</sub> photocatalyst.

the model. The temporal UV-vis spectral changes of RhB aqueous solution during the photocatalytic degradation reactions are depicted in Figure 8. As seen from the figure, when the RhB solution was irradiated with the high-pressure Hg lamp, the main RhB absorbance markedly decreased with irradiation time and almost completely disappeared after 80 min of irradiation. Comparison experiments demonstrated that RhB photolysis (without any catalyst) was very slow and that RhB could not be degraded in the presence of Fe<sub>3</sub>O<sub>4</sub>/TiO<sub>2</sub> hybrid catalyst under the dark conditions, signifying that RhB degradation in the present study is indeed through a photocatalytic process. Furthermore, it was observed that the main absorbance of RhB (at 554 nm) gradually shifted to shorter wavelength and reached 496 nm at 40 min of irradiation; after that time the peak position did not change, whereas the peak intensity further decreased to 0 at 80 min of irradiation. The hypsochromic shift in  $\lambda_{\max}$  of RhB over Fe<sub>3</sub>O<sub>4</sub>/TiO<sub>2</sub> hybrid catalyst may be due to the step-by-step de-ethylation of RhB.<sup>30</sup> The peak centered at 496 nm was assigned to the absorbance of the completely de-ethylated product of RhB, namely rhodamine. The compounds that give absorption peaks between 496 and 554 nm might consist of several partially de-ethylated intermediates, including N,N,N'-triethylated rhodamine ( $\lambda_{\max}$  at 539 nm), N,N'-triethylated rhodamine ( $\lambda_{\max}$  at 522 nm), and N'-triethylated rhodamine ( $\lambda_{\max}$  at 510 nm).<sup>31</sup> The gradual shift in  $\lambda_{\max}$  indicates that the de-ethylation reaction proceeded in a stepwise manner. The reduction in the absorbance after the completion of N-triethylation was due to the subsequent degradation reaction. Compared to previously reported TiO<sub>2</sub> hollow spheres, the photocatalytic activity of our magnetic photocatalyst is weaker, which may be in response to the hybrid composition.<sup>20</sup> However, it shows

higher activity than the solid TiO<sub>2</sub> spheres<sup>32</sup> and P25. In this system, the real photocatalytic mechanism of the magnetic catalyst is still not clear, and further work should be done.

The magnetic property of the Fe<sub>3</sub>O<sub>4</sub>/TiO<sub>2</sub> hybrid composite is useful for efficient recovery and recycling of magnetic photocatalysts in liquid-phase reactions. As an example, when the Fe<sub>3</sub>O<sub>4</sub>/TiO<sub>2</sub> hollow spheres were dispersed in water giving a black suspension, upon applying an external magnetic field, the black powder was readily harvested within 30 s and the solution became transparent (Figure S3 in the Supporting Information). As a recyclable photocatalyst, another important factor, renewable photocatalytic activity, was also investigated. The result is shown in Figure 8, from which we can see that decreased after six cycles of the photocatalysis experiment. With the increase of cycle times, the reaction time was prolonged. However, the decolorization efficiency was still up to 89.6% in the sixth cycle. In conclusion, as-prepared Fe<sub>3</sub>O<sub>4</sub>/TiO<sub>2</sub> hollow spheres have good photocatalytic activity in degradation of RhB in aqueous solution and this catalytic activity can maintain 93% photocatalysis activity after being reused six times. The decrease of the catalytic activity after each recycling may partly result from incomplete magnetic separation of the catalyst.

#### 4. Conclusions

In summary, magnetically separable photocatalysts with hollow nanostructure have been fabricated through a PSA template method. These Fe<sub>3</sub>O<sub>4</sub>/TiO<sub>2</sub> hollow spheres were synthesized in a stepwise process. First, PSA latexes were coated by a noncontinuous layer of Fe<sub>3</sub>O<sub>4</sub> via an in situ deposition method. Next, a denser amorphous TiO<sub>2</sub> shell encapsulated the initial magnetic PSA spheres. Finally, the Fe<sub>3</sub>O<sub>4</sub>/TiO<sub>2</sub> hollow particles can be obtained after the PSA etching and solvothermal treatment. These hollow spheres of 400 nm size show superparamagnetic and good photocatalytic properties, for they are comprised of nanosized TiO<sub>2</sub> and Fe<sub>3</sub>O<sub>4</sub>. The combination of the photocatalysis properties of TiO<sub>2</sub> and the superparamagnetic property of Fe<sub>3</sub>O<sub>4</sub> nanoparticles endows this material with a bright perspective in purification of polluted wastewater. Moreover, this work also provided a facile and general method for synthesizing nanocomposites of magnetic Fe<sub>3</sub>O<sub>4</sub> and other functional nanoparticles, which may find wider applications besides in catalysis.

**Supporting Information Available:** Figure S1 showing FTIR spectra of PSA, PSA@Fe<sub>3</sub>O<sub>4</sub>, and PSA@Fe<sub>3</sub>O<sub>4</sub>/Ti(OH)<sub>x</sub> spheres; Figure S2 showing TG curves of PSA@Fe<sub>3</sub>O<sub>4</sub> and PSA@Fe<sub>3</sub>O<sub>4</sub>/Ti(OH)<sub>x</sub> spheres; Figure S3 showing magnetic separation of the magnetic photocatalyst. This material is available free of charge via the Internet at <http://pubs.acs.org>.

#### References and Notes

- (1) Tang, J.; Zou, Z.; Ye, J. *Angew. Chem., Int. Ed.* **2004**, *43*, 4463.
- (2) Fox, M. A.; Dulay, M. T. *Chem. Rev.* **1993**, *93*, 341.
- (3) Heller, A. *Acc. Chem. Res.* **1995**, *28*, 503.
- (4) Nakajima, A.; Obata, H.; Kameshima, Y.; Okada, K. *Catal. Commun.* **2005**, *6*, 716.
- (5) Zhang, L.; Zhu, Y.; He, Y.; Li, W.; Sun, H. *Appl. Catal., B* **2003**, *40*, 287.
- (6) (a) Liu, S. M.; Gan, L. M.; Liu, L. H.; Zhang, W. D.; Zeng, H. C. *Chem. Mater.* **2002**, *14*, 1391. (b) Zhang, L.; Yu, J. C. *Chem. Commun.* **2003**, 2078. (c) Shibata, H.; Ogura, T.; Mukai, T.; Ohkubo, T.; Sakai, H.; Abe, M. *J. Am. Chem. Soc.* **2005**, *127*, 16396. (d) Yuan, Z. Y.; Ren, T. Z.; Vantomme, A.; Su, B. L. *Chem. Mater.* **2004**, *16*, 5096.
- (7) (a) Luo, H.; Wang, C.; Yan, Y. *Chem. Mater.* **2003**, *15*, 3841. (b) Zhou, Y.; Antonietti, M. *J. Am. Chem. Soc.* **2003**, *125*, 14960. (c) Blin, J. L.; Leonard, A.; Yuan, Z. Y.; Gigot, L.; Vantomme, A.; Cheetham, A. K.; Su, B. L. *Angew. Chem., Int. Ed.* **2003**, *42*, 2872.

- (8) (a) Yun, H. S.; Miyazawa, K.; Zhou, H.; Honma, I.; Kuwabara, M. *Adv. Mater.* **2001**, *13*, 1377. (b) Yuan, Z. Y.; Ren, T. Z.; Su, B. L. *Adv. Mater.* **2003**, *15*, 1462. (c) Wang, K.; Yao, B.; Morris, M. A.; Holmes, J. D. *Chem. Mater.* **2005**, *17*, 4825. (d) Shibata, H.; Ogura, T.; Mukai, T.; Ohkubo, T.; Sakai, H.; Abe, M. *J. Am. Chem. Soc.* **2005**, *127*, 16396. (e) Kirsch, B. L.; Richman, E. K.; Riley, A. E.; Tolbert, S. H. *J. Phys. Chem. B* **2004**, *108*, 12698.
- (9) Zhan, S. H.; Chen, D. R.; Jiao, X. L.; Tao, C. H. *J. Phys. Chem. B* **2006**, *110*, 11199.
- (10) Pozzo, R. L.; Martin, S. T.; Choi, W.; Bahnemann, D. *Chem. Rev.* **1995**, *95*, 69.
- (11) Arai, T.; Sato, T.; Kanoh, H.; Kaneko, K.; Oguma, K.; Yanagisawa, A. *Chem.—Eur. J.* **2008**, *14*, 882.
- (12) Yoon, H.; Ko, S.; Jang, J. *Chem. Commun.* **2007**, 1468–1470.
- (13) Yi, D. K.; Lee, S. S.; Ying, J. Y. *Chem. Mater.* **2007**, *18*, 2459.
- (14) Shokouhimehr, M.; Piao, Y. Z.; Kim, J. Y.; Jang, Y. J.; Hyeon, T. W. *Angew. Chem., Int. Ed.* **2007**, *46*, 7039.
- (15) Beydoun, D.; Amal, R.; Low, G. K. C.; Mcevoy, S. J. *J. Phys. Chem. B* **2000**, *104*, 4387.
- (16) Zhang, B. P.; Zhang, J. L.; Chen, F. *Res. Chem. Int.* **2008**, *34*, 375.
- (17) Lee, S. W.; Drwiega, J.; Wu, C. Y.; Mazyck, D.; Sigmund, W. M. *Chem. Mater.* **2004**, *16*, 1160.
- (18) Gad-Allah, T. A.; Kato, S.; Satokawa, S.; Kojima, T. *Solid State Sci.* **2007**, *9*, 737.
- (19) Caruso, F. *Adv. Mater.* **2001**, *13*, 11.
- (20) Li, X. X.; Xiong, Y. J.; Li, Z. Q.; Xie, Y. *Inorg. Chem.* **2006**, *45*, 3493.
- (21) (a) Zhang, K.; Zhang, X. H.; Chen, H. T.; Chen, X.; Zheng, J. L.; Zhang, J. H.; Yang, B. *Langmuir* **2004**, *20*, 11312. (b) Li, H. X.; Bian, Z. F.; Zhu, J.; Zhang, D. Q.; Li, G. S.; Huo, Y. N.; Li, H.; Lu, Y. F. *J. Am. Chem. Soc.* **2007**, *129*, 8406.
- (22) Mu, G. H.; Pan, X. F.; Chen, N.; He, C. H.; Gu, M. Y. *Appl. Surf. Sci.* **2008**, *254*, 2483.
- (23) Carsuo, F. *Chem.—Eur. J.* **2000**, *6*, 413.
- (24) Imhof, A. *Langmuir* **2001**, *17*, 3579.
- (25) Chen, B.; Zhu, Y.; Jiang, W.; Chen, Z.; Wang, C.; Zhou, G.; Zhang, P. *J. Nanopart. Res.* **1999**, *1*, 491.
- (26) Yang, Z.; Niu, Z.; Lu, Y.; Hu, Z.; Han, C. C. *Angew. Chem., Int. Ed.* **2003**, *42*, 1943.
- (27) Huang, Z. B.; Tang, F. Q. *J. Colloid Interface Sci.* **2004**, *275*, 142.
- (28) Chen, X. B.; Burda, C. *J. Phys. Chem. B* **2004**, *108*, 15446.
- (29) Han, D. H.; Wang, J. P.; Luo, H. L. *J. Magn. Magn. Mater.* **1994**, *36*, 176.
- (30) Li, X. K.; Ye, J. H. *J. Phys. Chem. C* **2007**, *111*, 13109.
- (31) Watamane, T.; Takirawa, T.; Hidaka, M.; Rakhmawaty, D.; Anpo, M. *J. Catal.* **2007**, *246*, 235.
- (32) Xu, H.; Jia, F. L.; Ai, Z. H.; Zhang, L. Z. *Cryst. Growth Des.* **2007**, *7*, 1216.

JP8073859